

Electronic Supplementary Information (ESI)

Consumer-grade polyurethane foam functions as a large and selective absorption sink for bisphenol A in aqueous media

Jie Han,^{a,†} Wei Qiu,^a Saumya Tiwari,^b Rohit Bhargava,^b Wei Gao,^c and Baoshan Xing^{a,†}

^a Stockbridge School of Agriculture, University of Massachusetts, Amherst, Massachusetts 01003, United States.

^b Department of Bioengineering and Beckman Institute for Advanced Science and Technology, University of Illinois at Urbana-Champaign, Urbana, Illinois 61801, United States.

^c Department of Chemical and Materials Engineering, The University of Auckland, Auckland 1010, New Zealand.

18 pages, excluding cover page.

11 figures

5 tables

Submitted to *Journal of Materials Chemistry A*

[†]Corresponding authors. Jie Han, jiehan@umass.edu; Baoshan Xing, bx@umass.edu.

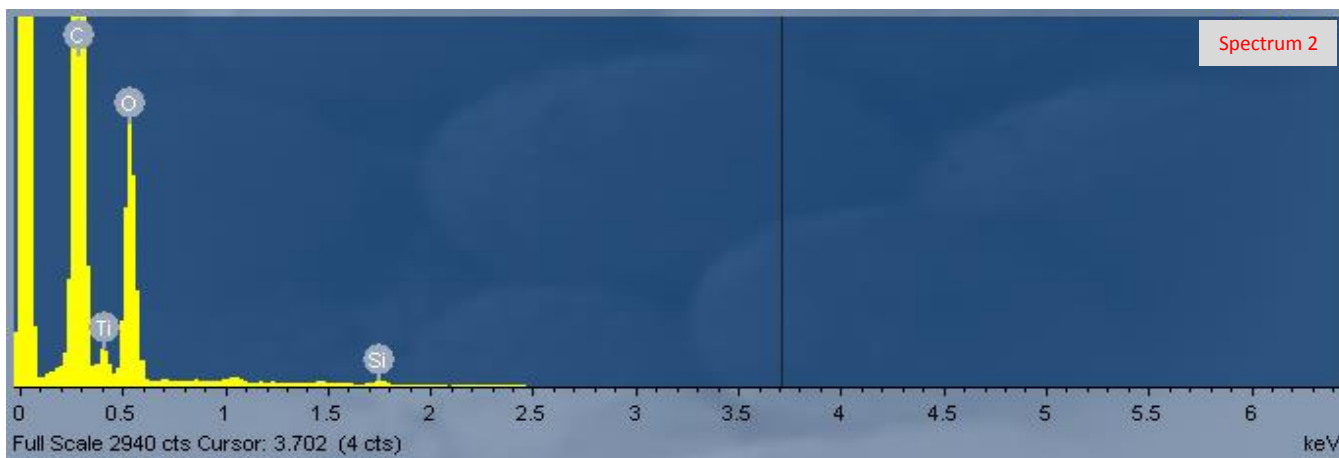
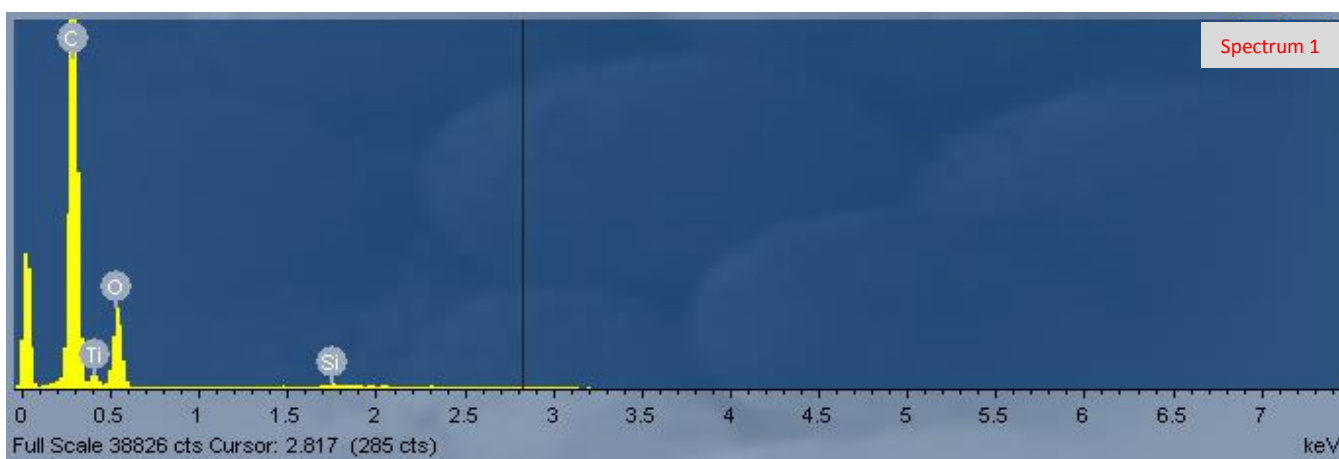
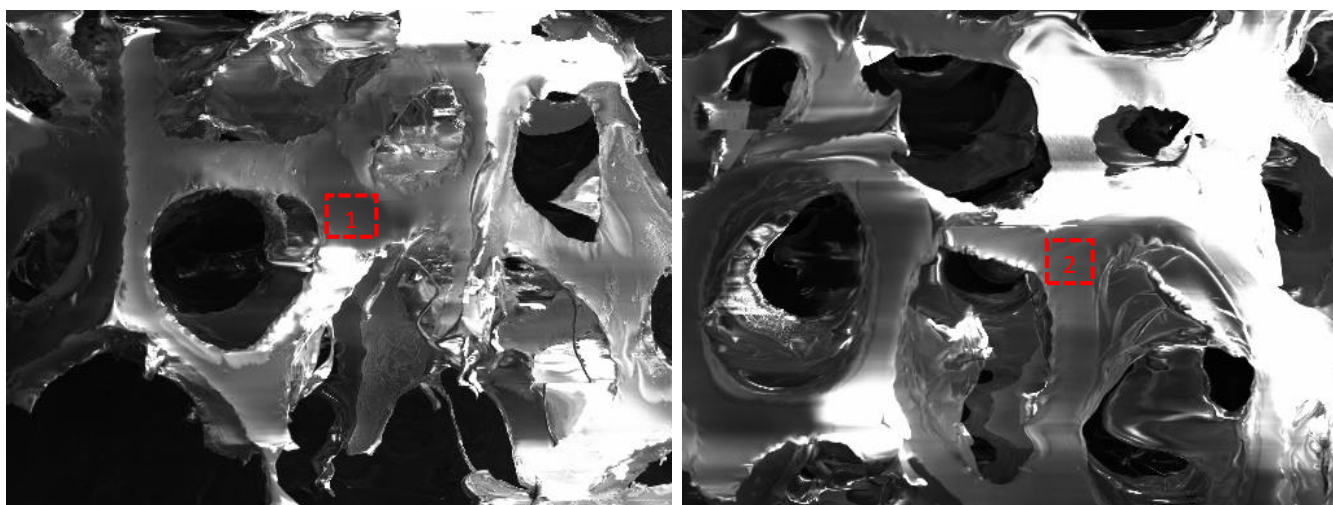
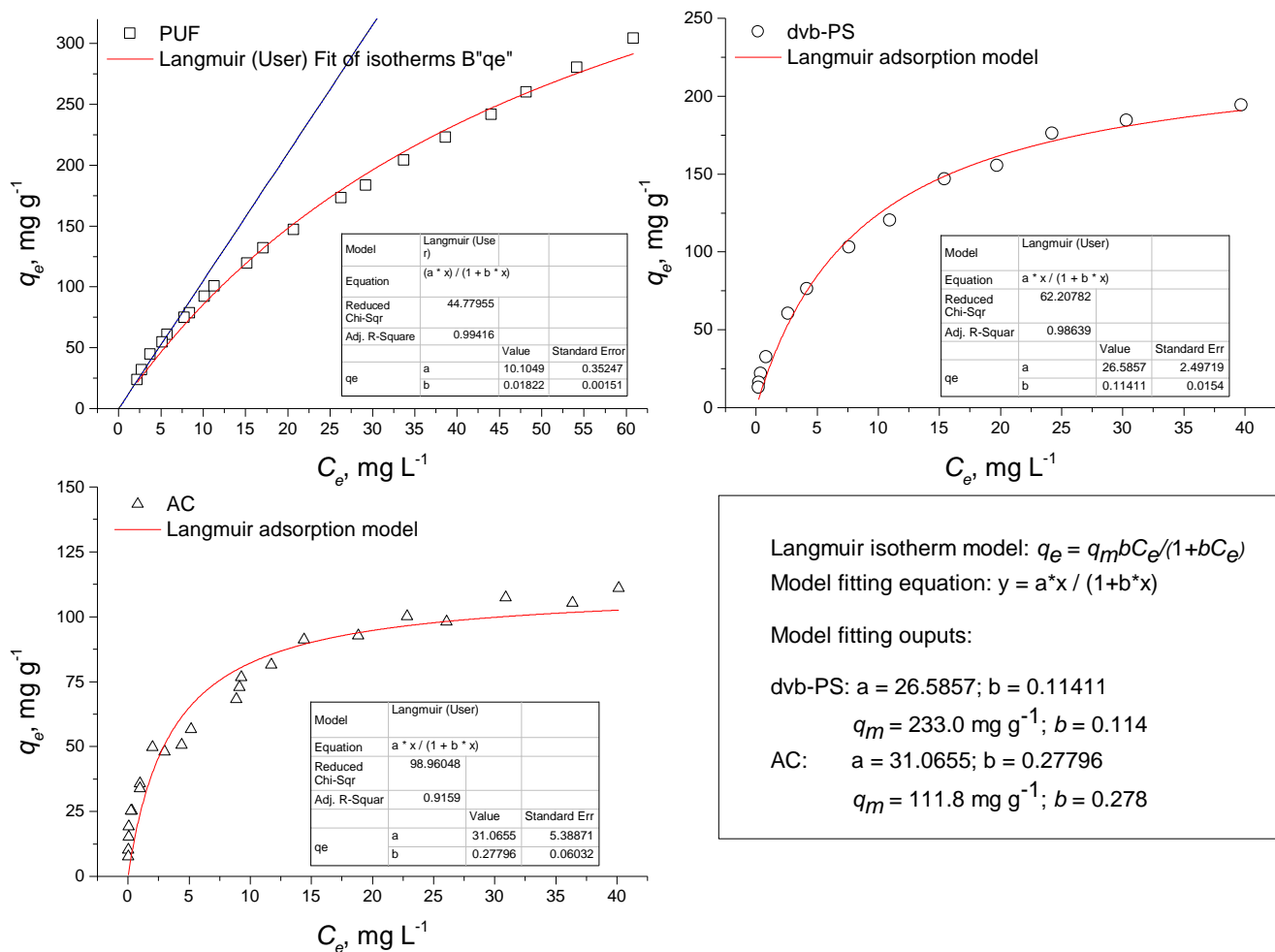


Figure S1. Scanning electron microscope (SEM) images and energy dispersive X-ray spectra (EDS) of a pristine specimen of the reference PUF. Analyses were performed on a FEI Magellan 400 High-Resolution Scanning Electron Microscope. EDS spectra were acquired under 5.0 kV acceleration voltage and 6.4 nA current from user-selected regions on SEM images of PUF fibrils under 500x magnification. The small amount of Ti detected was likely to be from the titanium oxide pigments dosed into the material during the manufacturing process. The trace amount of silicone (Si) was likely due to contamination by air dusts during the sample preparation and handling.



Langmuir isotherm model: $q_e = q_m b C_e / (1 + b C_e)$
 Model fitting equation: $y = a * x / (1 + b * x)$

Model fitting outputs:

dvb-PS: $a = 26.5857$; $b = 0.11411$
 $q_m = 233.0 \text{ mg g}^{-1}$; $b = 0.114$

AC: $a = 31.0655$; $b = 0.27796$
 $q_m = 111.8 \text{ mg g}^{-1}$; $b = 0.278$

Figure S2. BPA sorption isotherm data fitted to Langmuir adsorption model by NLLS regression. Insets show data fitting reports and derived model parameters. Data plotting and model fitting were performed in Origin 9.1 (OriginLab, MA) under an Academic Use License. The Langmuir isotherm model is a theoretical equation based on the assumptions of reversible surface adsorption, monolayer adsorption, and limited adsorption sites. The model can be expressed by the equation $q_e = q_m b C_e / (1 + b C_e)$, where q_e (mg g^{-1}) represents the amount of solute sorbed by per unit weight of sorbent at equilibrium; C_e (mg L^{-1}) represents the equilibrium concentration of solute compound; q_m (mg g^{-1}) represents the theoretical maximum sorption capacity of the sorbent; and b ($\text{L}^{-1} \text{ mg}$) is a constant indicative of binding energy. Fitting to the linear partitioning model was done in the low-concentration region ($C_e < 10 \text{ mg L}^{-1}$) on a trial-and-error basis using simulated curves generated by Origin 9.1. The linear plot displayed in PUF sorption isotherm graph follows the equation $q_e = 10.5 C_e$.

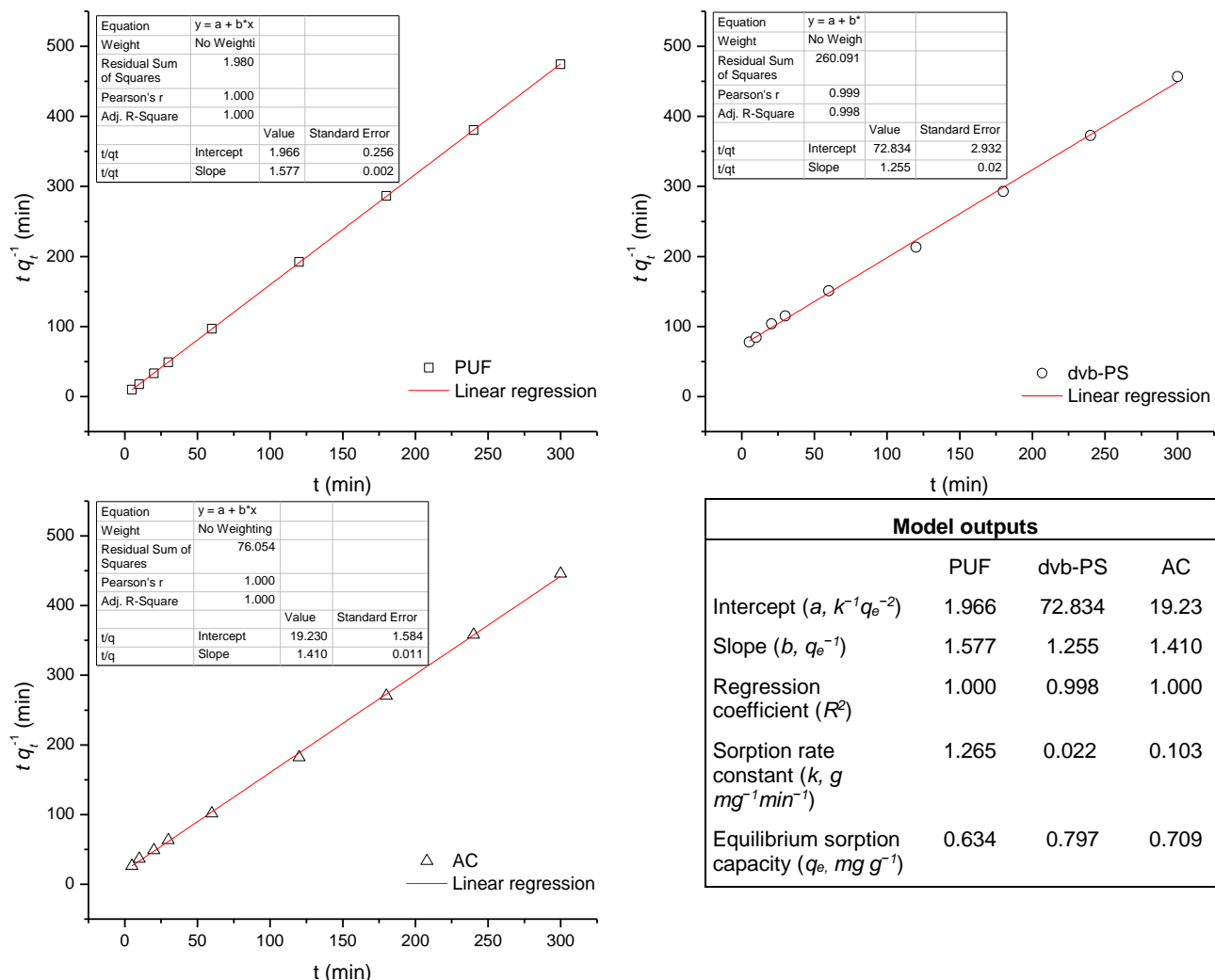


Figure S3. BPA sorption kinetic data fitted to the pseudo-second-order (PSO) kinetic model. Data fitting reports are shown in the figure insets and the derived model parameters are summarized in the table inset. The PSO kinetics model describes reversible adsorption on liquid/solid interface in aqueous media at low sorbate concentrations relative to the sorbent dosage applied.¹ The model can be expressed by $t/q_t = 1/kq_e^2 + t/q_e$, where t (min) is accumulative sorption time; k ($\text{g mg}^{-1} \text{ min}^{-1}$) is rate constant; q and q_e (mg g^{-1}) are sorbate uptake by per unit weight of sorbent at a particular time (t) and equilibrium, respectively. The theoretical analysis and mathematical derivation of the PSO model are available in literature.¹ The intercept (a) and slope (b) of fitted curve correspond to $1/kq_e^2$ and $1/q_e$ in the PSO model equation, respectively. Sorption rate constant (k) and equilibrium sorption capacity (q_e) are determined by $k = b^2/a$ and $q_e = 1/b$, respectively.

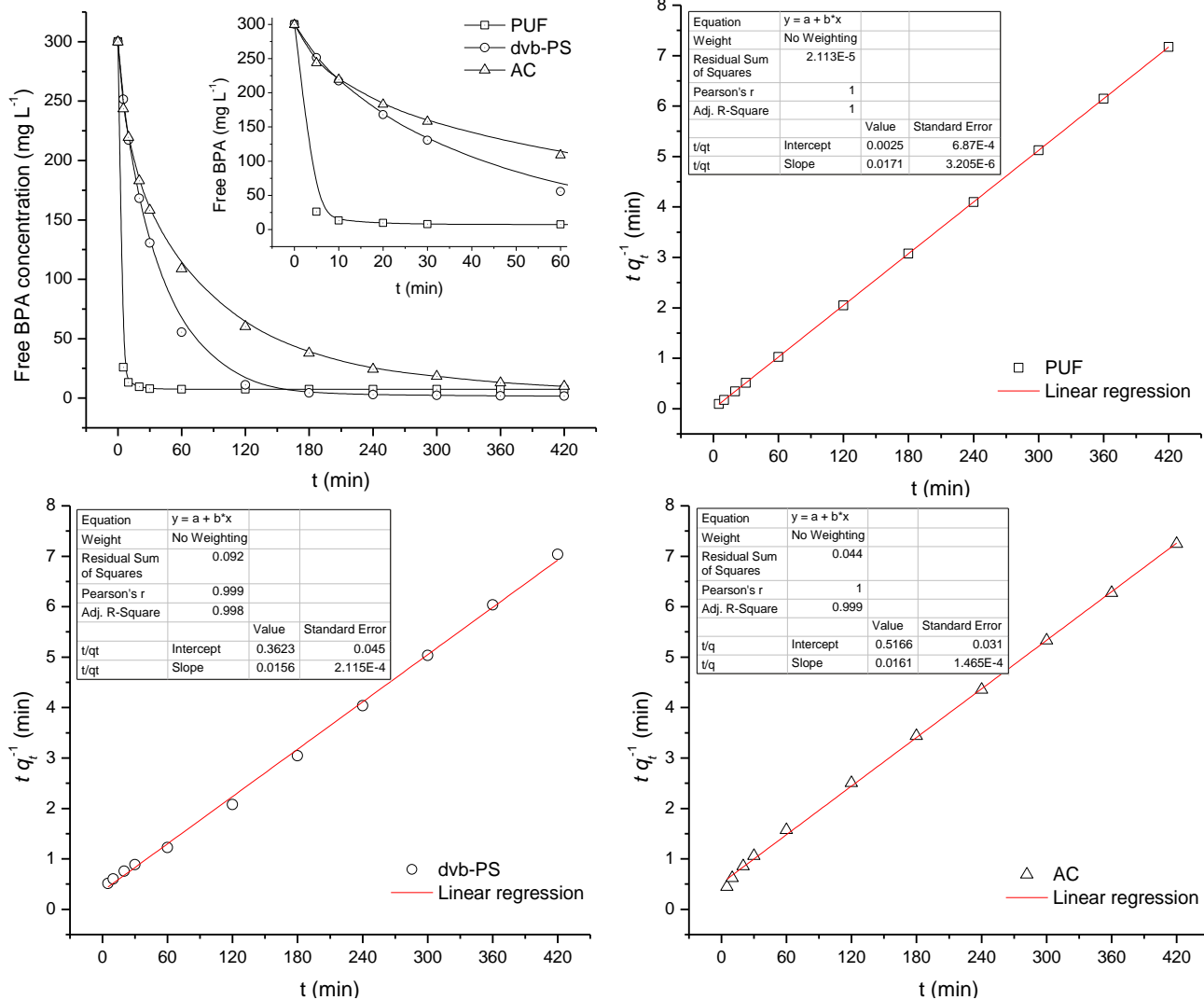


Figure S4. BPA sorption kinetics under an initial concentration of 300 mg L⁻¹ and data fitting to the PSO kinetic model. Conditions: initial [BPA]: 300 mg L⁻¹; sorbent dosage (dry weight basis): 5.0 g L⁻¹; 225 rpm agitation, at 20 ± 0.5°C. Table insets show data fitting reports and derived model parameters. The second-order rate constant (k , g mg⁻¹ min⁻¹) follows the order of PUF (0.12) > dvb-PS (6.7×10⁻⁴) > AC (5.0×10⁻⁴). Note that the BPA uptake rate by PUF is two magnitudes (180–240 fold) higher than the equivalent rates obtained by dvb-PS and AC. The difference in their uptake rates widened under the high initial BPA concentration by comparing with the results in Figure 1c.

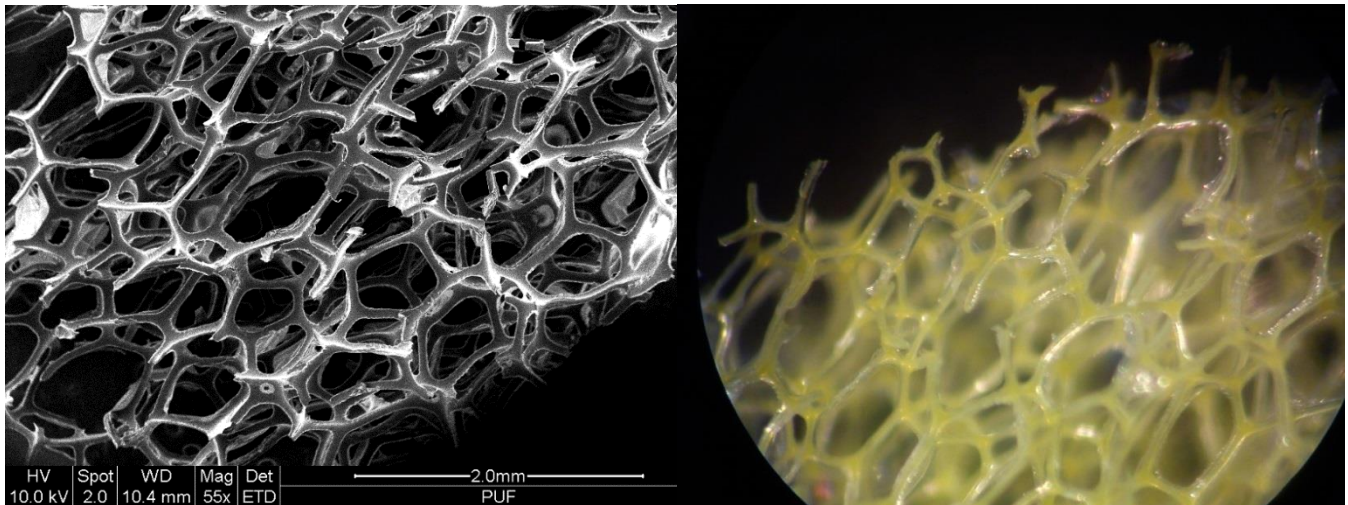


Fig. 2a. Fibril skelton and open cells in PUF

Fig. 2a inset. Fibril skelton and open cells in PUF (optical microscope image)

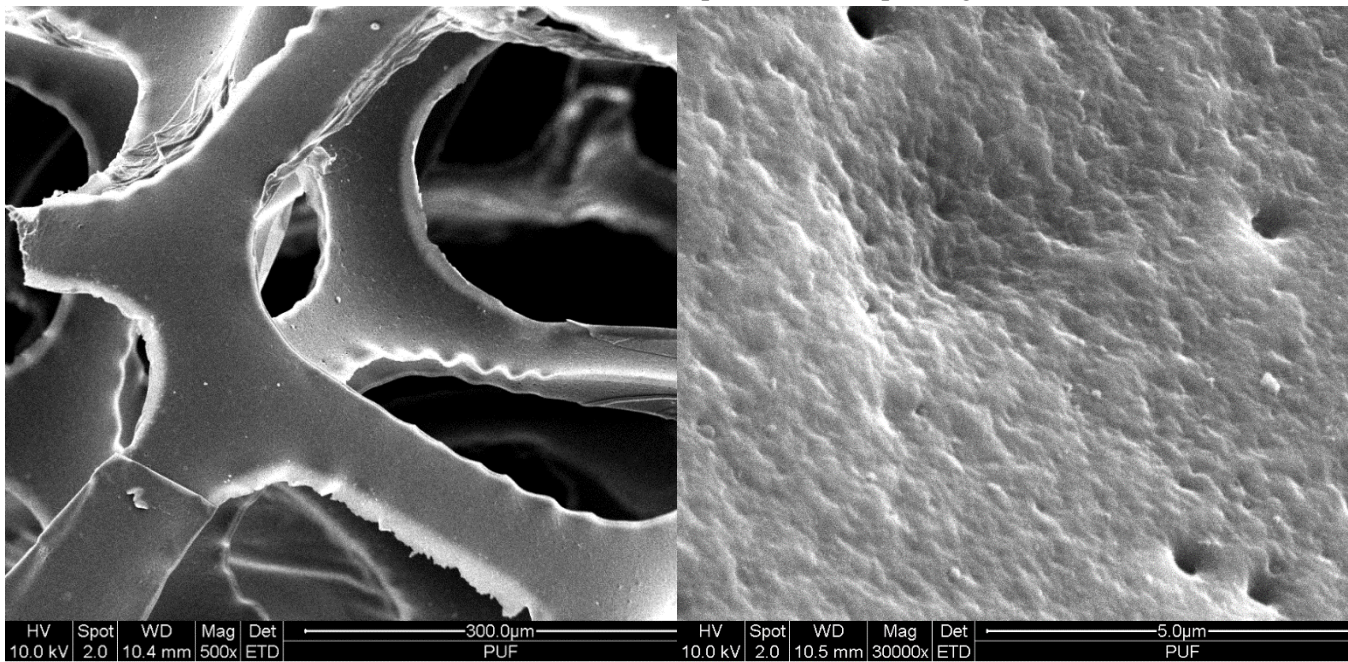


Fig. 2b. Pristine PUF fibrils

Fig. 2b inset. Typical surface morphology of pristine PUF fibril

(cont.)

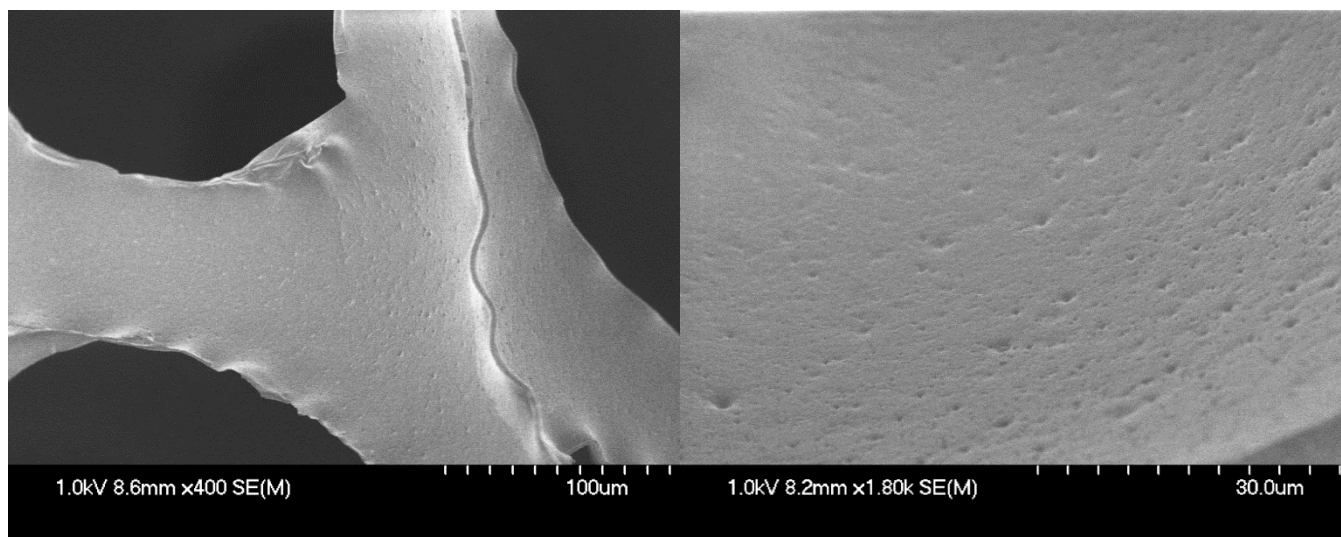


Fig. 2c. BPA-laden PUF fibril (PUF-BPA_{0.4})

Fig. 2c inset. Surface morphology of BPA-laden PUF fibril (PUF-BPA_{0.4})

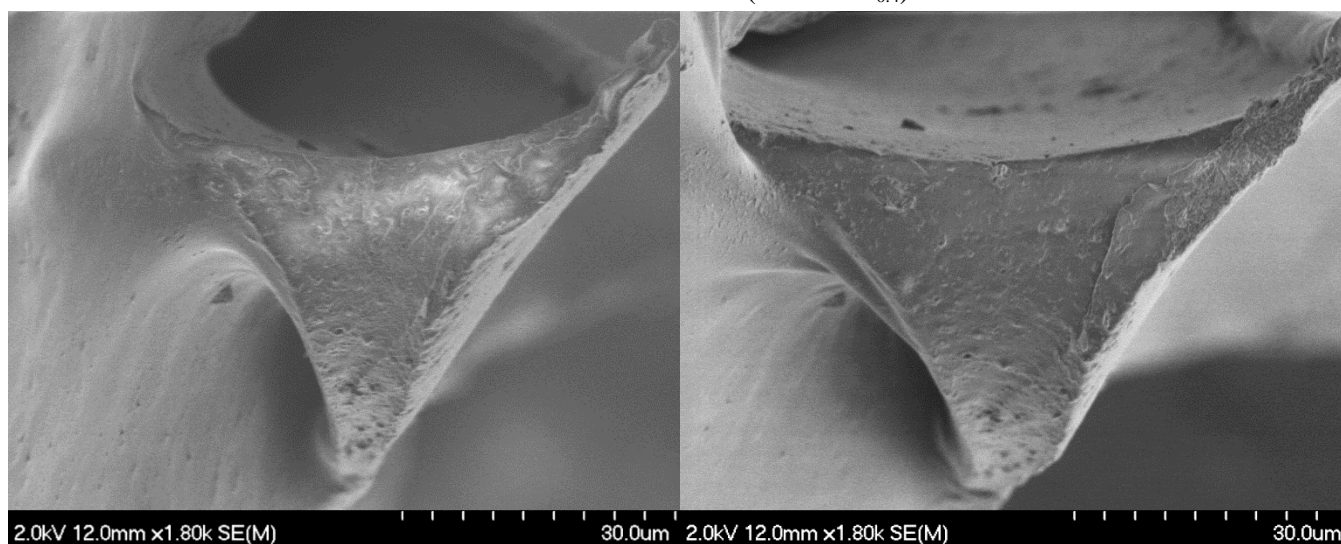


Fig. 2d. Cross-section of a pristine PUF fibril

Fig. 2e. Cross-section of the same PUF fibril (PUF-BPA_{0.4}) after large BPA uptake

Figure S5. Original optical and electron microscope images of pristine and BPA-laden PUF fibrils. For cross-referencing, images are numbered and arranged in the same order as appeared in Figure 2. Images 2d and 2e were acquired on a single, free-standing fibril isolated from the PUF-BPA_{0.4} specimen using a Hitachi S4700 HR-FESEM under identical instrumental settings, *i.e.* accelerating voltage: 2.0 kV, working distance: 12.0 mm, and magnification: 1.80 k. The working distance is the distance between the bottom face of objective lens and the focal point on the surface of the specimen analyzed.²

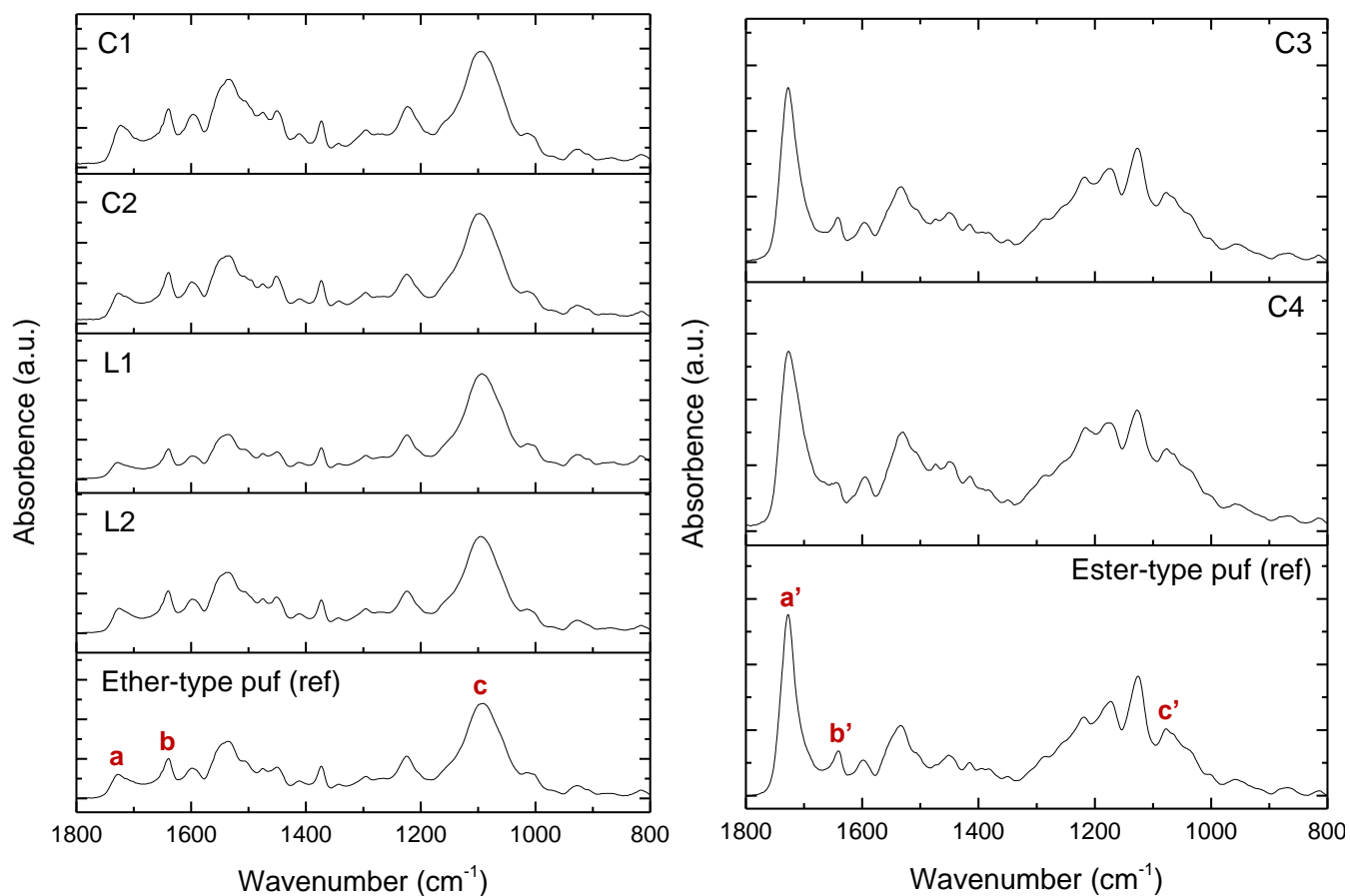


Figure S6. Fourier-transform infrared spectra of the six PUF materials studied for PUF fibril swelling. Reference spectra (ref) show the infrared spectra of standard polyether-type and polyester-type PUFs, which are distinguished by the large IR absorption band centered at 1745 cm^{-1} that is characteristic to ester carbonyl stretching, and the IR absorption band at 1090 cm^{-1} that is characteristic to ether carbonyl stretching. Assignments of the peaks labeled in reference spectra: (a) urea/urethane carbonyl stretching; (b) urea carbonyl stretching; (c) ether C–O–C stretching; (a') ester carbonyl stretching (main), urea/urethane carbonyl stretching (minor); (b') urea carbonyl stretching; and (c') ester C–O stretching. Infrared bands of PUF and their assignments are discussed in detail in ref 3, and more broadly in ref 4. Spectra were acquired under the attenuated total reflectance (ATR) mode using a Diamond/ZnSe crystal on a PerkinElmer SpectrumOne FTIR spectrometer at a spectral resolution of 4 cm^{-1} with signal averaging from 64 scans. The ATR mode particularly suited for analyzing deformable PUF materials.⁵ After data acquisition, each raw spectrum was processed by ATR correction and baseline correction using the built-in data processing program, SpectrumOne Suite.

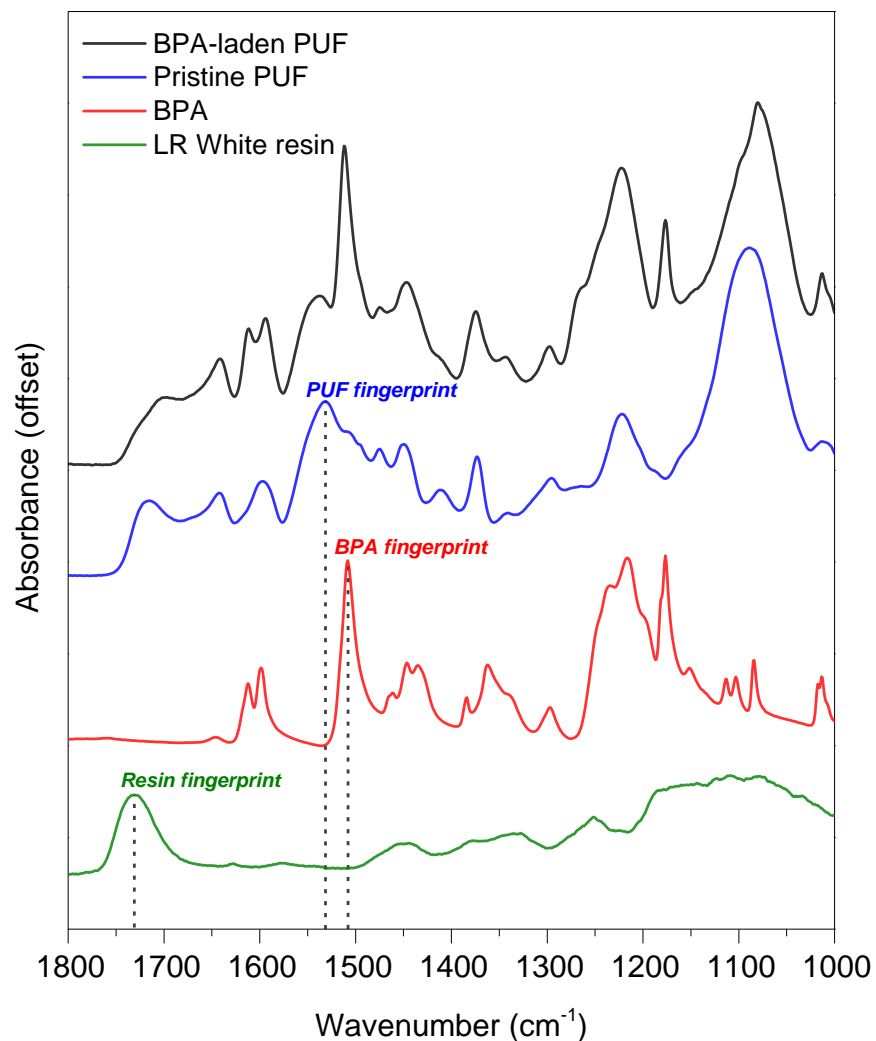


Figure S7. Identification of fingerprint peaks in BPA-laden PUF fibrils embedded in LR White resin. The stacked graph above shows the Fourier-transform infrared spectra of BPA-laden PUF (PUF-BPA_{0.4}), pristine PUF, BPA, and LR White resin from top to bottom. Fingerprint peaks were selected from major characteristic infrared absorption bands of the target material or compound with the additional criterion of having low signal interferences from co-existing material or compound.

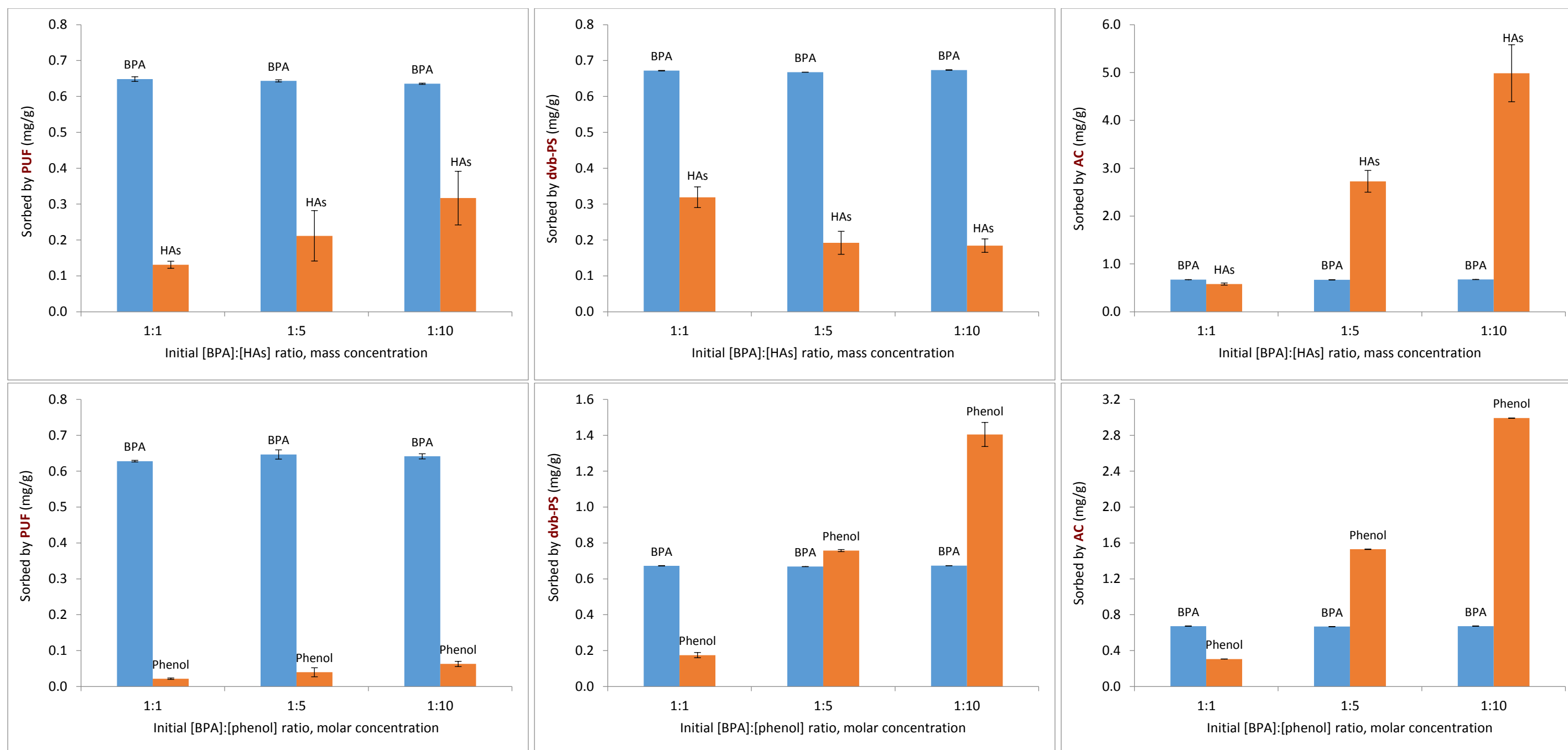


Figure S8. Breakdown graphs showing the sorption selectivity of PUF, dvb-PS, and AC for BPA against co-existing NOM and SSC, *i.e.* humic acids (HAs) and phenol. Each graph shows the result of triplicate experiments. HPLC analysis confirmed that residual BPA was non-detectable ($< 1.0 \mu\text{g L}^{-1}$) after sorption equilibrium was reached using dvb-PS and AC at the dosage of 1.5 g L^{-1} , in which cases BPA was considered to be completely removed from the treated solutions. This yielded very low standard deviations in their triplicate results where the fluctuations of BPA uptake were only caused by minor variations in the sorbent dosages applied. Interferences of the trace amounts of preservative salt residues in dvb-PS resin were taken into account by subtracting their absorbance from the UV/Vis absorbance spectra of BPA/HAs solutions.

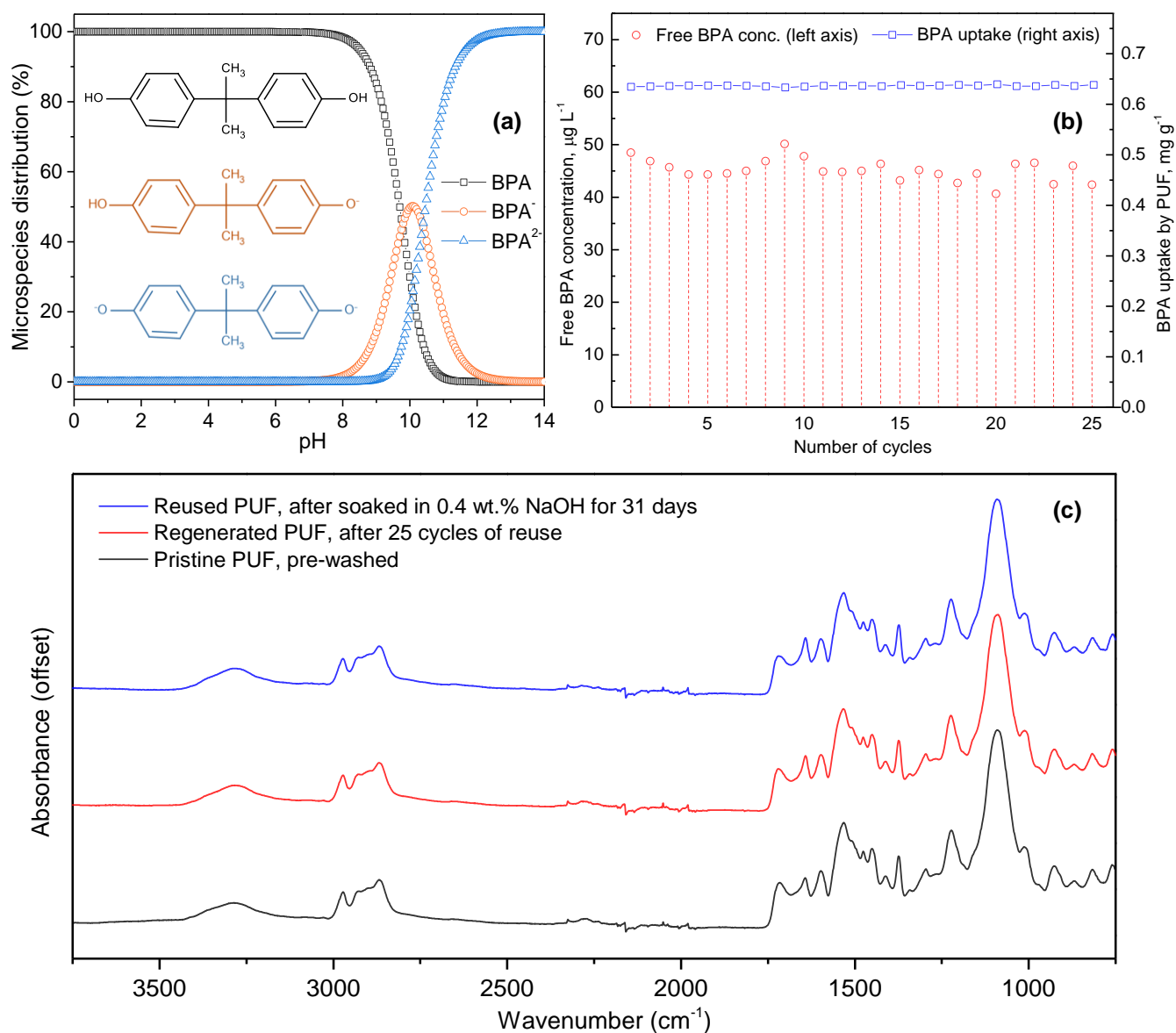


Figure S9. (a) Ionization of BPA solute in water as a function of pH. Ionization to divalent BPA²⁻ anion reaches 99.0% at pH 12.4. Quantitative structure–property relationship calculations were performed using ChemAxon Marvin Suite ver. 6.3.1. The increase of the aqueous solubility of BPA at alkaline pH was briefly reported in literature⁶. (b) BPA sorption results by using a pre-washed PUF specimen in 25 continuous cycles of BPA sorption and alkaline regeneration. A fresh BPA working solution (1.0 mg L⁻¹, 100 mL) was used at the beginning of each cycle. After sorption equilibrium was reached, the specimen was regenerated in two consecutive baths of 0.4 wt.% NaOH solutions, rinsed to pH neutral, and immediately used in the next cycle. Fluctuations in residual BPA concentration were likely due to minor differences in the initial solution used in each cycle and the measurement errors by HPLC. (c) Fourier transform infrared spectra of pristine PUF, regenerated PUF after 25 cycles of reuse, and the reused PUF after soaking in 0.4 wt.% NaOH for 31 days at room temperature. No spectral difference was identified in PUF characteristic infrared absorption bands after the multiple cycles of reuse or exposure to alkaline regenerant solution.

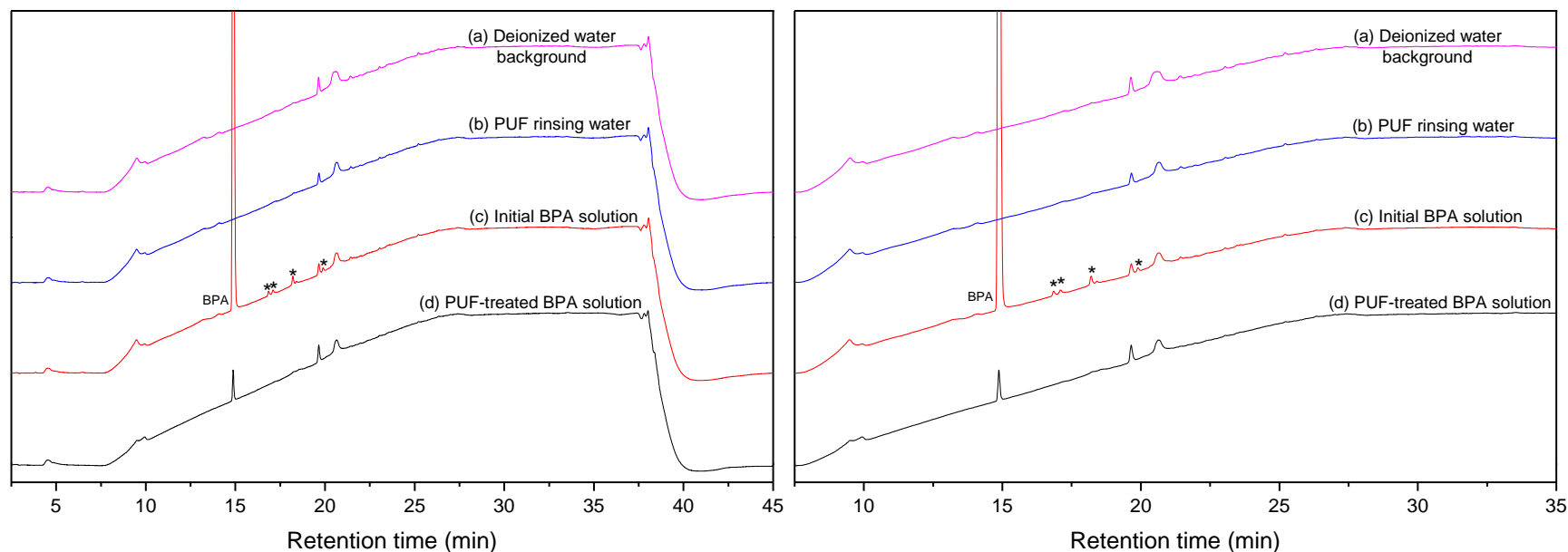


Figure S10. HPLC analysis of the potential release of monomers and oligomers by PUF. The graphs above show the gradient HPLC spectra of four control samples including (a) deionized water background, (b) PUF rinsing water, (c) initial BPA solution, and (d) PUF-treated BPA solution. The gradient method was developed to detect traces of monomers and oligomers potentially released from PUF during the 24-h exposure to water (sample b) and the BPA sorption process (sample d). Using this method, each sample was first analyzed with 20% of acetonitrile (ACN) in the mobile phase for 5 min ($t = 0\text{--}5$ min). Then the percentage of ACN in the mobile phase increased from 20% to 95% over a course of 20 min ($t = 5\text{--}25$ min). This was followed by another 10-min analysis with 95% ACN ($t = 25\text{--}35$ min). This method was to separate different compounds in samples that may have similar retention times in a C18 HPLC column. Samples of deionized water (sample a) and initial BPA solution (sample c) were analyzed to provide reference spectra for identifying PUF monomer and oligomers in samples (b) and (d), respectively. PUF rinsing water was obtained by immersing a pre-washed PUF block (0.15 g) in 100 mL deionized water for 24 h under agitation. PUF-treated BPA solution (sample d) was obtained by equilibrating the small PUF block in 100 mL BPA working solution (1.0 mg L^{-1}) for 24 h under agitation. Using this method, the initial BPA solution (sample c) showed 4 peaks of impurity compounds in its HPLC spectrum (labeled with asterisks) due to the impurities in the BPA solids ($\geq 99\%$, Sigma-Aldrich). The HPLC spectra of PUF rinsing water and PUF-treated BPA solution showed no additional peak compared to their reference spectra. Further extension of the analysis time using 95% ACN to 40 min also revealed no additional peaks in their HPLC spectra (data not shown for brevity). Within the analytical detectability of HPLC using the gradient method, we did not find any identifiable monomers or oligomer compounds released from PUF under those control environments.

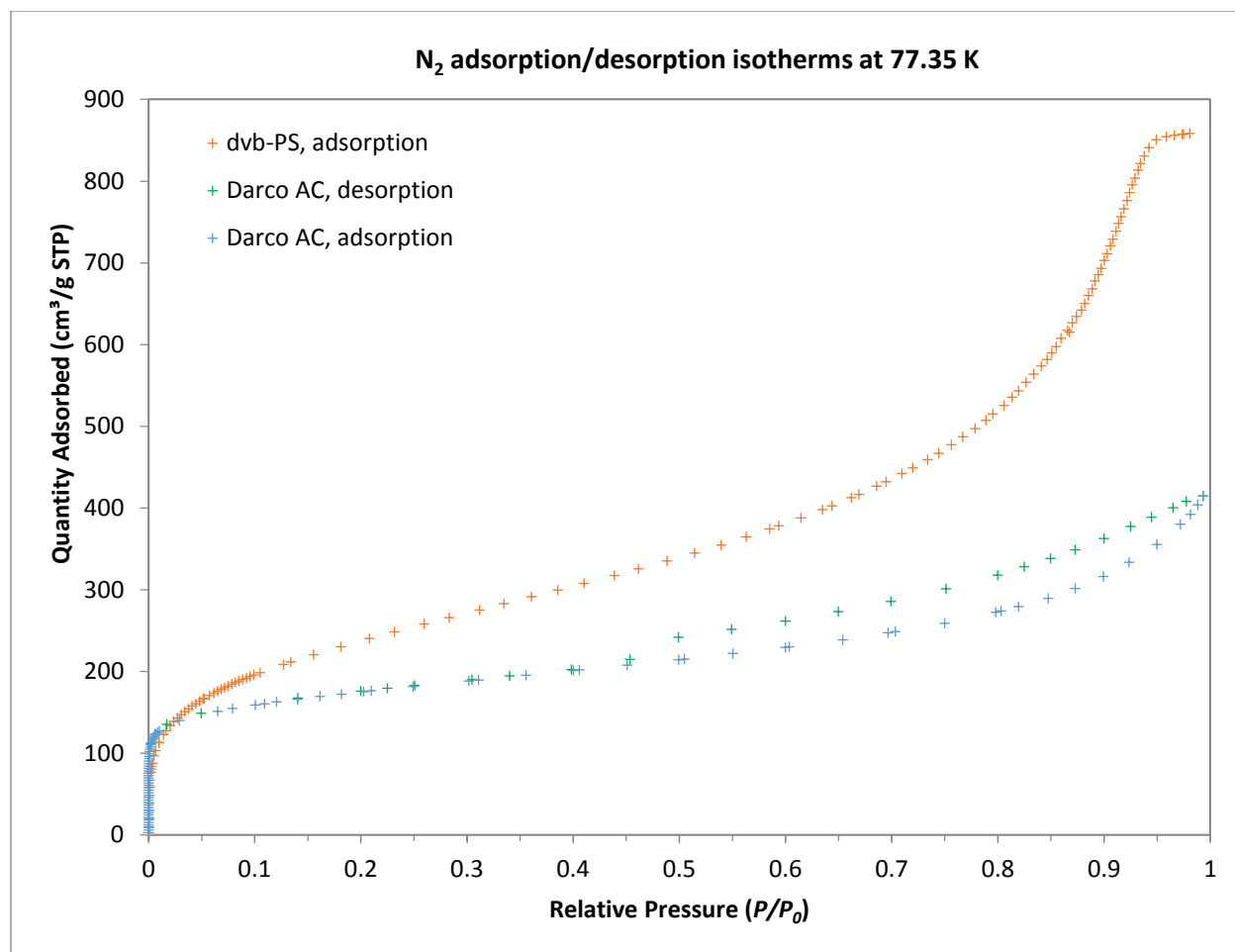



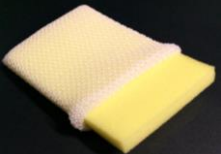
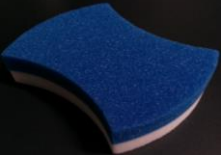



Figure S11. Nitrogen adsorption/desorption isotherms of AC and dvb-PS. Data were acquired by nitrogen adsorption at 77.35 K and used to determine the BET surface areas of AC and dvb-PS. Refer to Table S1 notes for details on experimental conditions.

Table S1. Physical properties of the reference PUF material and the benchmark dvb-PS and AC adsorbents

	<i>PUF</i>	<i>dvb-PS</i>	<i>AC</i>
Source	Consumer-grade material, 3M	Amberlite™ XAD4, Dow Chemical	Darco® 12×20, Cabot Norit
Material	Polyether-type polyurethane	Styrene-divinyl benzene copolymer	Carbon, activated
Morphology	Flexible foam with fibrils and open cells	Macroreticular microspheres	Porous granules
Particle size, mm	N/A	0.25–0.84 (datasheet)	0.85–1.70 (datasheet)
Specific surface area, m² g⁻¹	2.81 (exp.)	725 (datasheet); 841.3 (exp.)	650 (datasheet); 613.4 (exp.)
Total pore volume, cm³ g⁻¹	3.9×10 ⁻⁴ (exp.)	0.98 (datasheet); 1.06 (exp.)	0.95 (datasheet); 0.52 (exp.)
Average pore diameter, Å	N/A	50 (datasheet); 74 (exp.)	65 (exp.)

Notes: The physical properties of PUF, dvb-PS and AC are shown as their manufacturers' data (datasheet)^{7,8} and the data experimentally obtained in this study (exp.). Specific surface areas and pore characteristics were measured by the Brunauer-Emmett-Teller method on a Micromeritics ASAP2020 surface area and porosity analyzer. Nitrogen adsorption isotherm data were acquired at 77.35 K and used for calculating specific surface areas, total pore volumes, and average pore sizes. The measured pore volumes of dvb-PS and AC represent the total volume of nitrogen-accessible pores within the diameter range of 1.7–300 nm. The dvb-PS and AC adsorbents have been widely used for water purification and wastewater decontamination and were used as the benchmark adsorbents in this study. The term “macroreticular” refers to the relatively large and controlled pore size of dvb-PS. Each grain of the dvb-PS is formed by numerous microbeads cemented together during the polymerization process, and the voids between those microbeads form the “pores” of dvb-PS. The most widely studied macroreticular adsorbent resins are the Amberlite™ XAD series, manufactured by Rohm and Haas (now Dow Chemical). It should be clarified that the Amberlite® XAD resins are often mistakenly referred to as ion exchange resins and confused with Amberlite ion exchange resins, *e.g.* CG, IRA, and IRC series. However, for XAD resins, adsorption on the surface is the basis for their separations and no ion exchange mechanisms are involved. The use of dvb-PS for organic pollutants removal, particularly the Amberlite™ XAD series, have been documented in several review articles.^{9,10} Darco® 12×20 AC is an acid washed granular activated carbon produced by steam activation of lignite coal. It is a general purpose activated carbon and frequently used for water purification for its high dechlorination efficiency and adsorption capacity for tastes, odors, and colors.⁸

Table S2. Details on the six types of PUF materials used for gravimetric and volumetric determination of PUF fibril swelling

<i>Specimen No.</i>	<i>Image^a</i>	<i>Material grade</i>	<i>Manufacturer</i>	<i>Product Name</i>	<i>Cell structure</i>	<i>Type^b</i>
<i>C1</i>		Consumer grade	3M	Scotch-Brite™	Open cell	Polyether-type polyurethane
<i>C2</i>		Consumer grade	3M	Scotch-Brite™	Open cell	Polyether-type polyurethane
<i>C3</i>		Consumer grade	3M	Scotch-Brite™	Open cell	Polyester-type polyurethane
<i>C4</i>		Consumer grade	3M	Perfect-It™	Open cell	Polyester-type polyurethane
<i>L1</i>		Laboratory grade	Restek	Raw PUF	Open cell	Polyether-type polyurethane
<i>L2</i>		Laboratory grade	Jaece Industries	Identi-Plug®	Open cell	Polyether-type polyurethane

Notes: (a) Visual inspection and UV-Vis spectroscopic analysis on colored PUF materials confirmed that their dye additives did not leach into the washing solvents or deionized water during the pre-washing, or BPA solutions and alkaline regenerants during sorption and desorption processes. (b) Four of the six PUF specimens (C1, C2, L1, and L2) were of polyether-type polyurethane and two (C3 and C4) were of polyester-type polyurethane as shown by ATR-FTIR analysis (see Figure S6).

Table S3. Comparison of our sorption data with previously investigated sorbent materials for BPA

<i>Sorbent material</i>	<i>Description</i>	<i>BET surface area (m² g⁻¹)</i>	<i>Pore characteristics</i>	<i>BPA uptake (experimental data)</i>	<i>Max. BPA sorption capacity (model predicted data)</i>	<i>Notable variations in experimental parameters</i>	<i>Ref</i>
PUF	Consumer-grade material, 3M.	2.81	Negligible	$C_e = 38.6 \text{ mg L}^{-1}$, $q_e = 222.8 \text{ mg g}^{-1}$; $C_e = 33.7 \text{ mg L}^{-1}$, $q_e = 204.1 \text{ mg g}^{-1}$.	427.3 mg g ⁻¹	Not applicable	This study
dvb-PS	Amberlite™ XAD4, Dow Chemical.	841.3	Avg. pore size: 7.4 nm; V_{pore} : 1.06 cm ³ g ⁻¹	$C_e = 39.7 \text{ mg L}^{-1}$, $q_e = 194.2 \text{ mg g}^{-1}$.	233.0 mg g ⁻¹	Not applicable	This study
AC	Darco® 12×20, Cabot Norit Activated Carbon.	613.4	Avg. pore size: 6.5 nm; total pore volume: 0.52 cm ³ g ⁻¹	$C_e = 40.2 \text{ mg L}^{-1}$, $q_e = 111.0 \text{ mg g}^{-1}$.	111.8 mg g ⁻¹	Not applicable	This study
Carbon nanotubes (CNTs)	As-grown and microwave-modified CNTs	78.2 (as-grown); 94.8 (modified)	Not available	$C_e = ca. 54 \text{ mg L}^{-1}$, $q_e = ca. 70 \text{ mg g}^{-1}$ (highest value), at pH 6 and 7°C.	69.93 mg g ⁻¹ (highest value, modified carbon nanotubes)	Controlled pH and temperatures. Highest q_e and q_m were based on data obtained at pH 6 and 7°C.	Kuo, 2009 ¹¹
CNTs and fullerene	Single-walled carbon nanotubes (SWCNT), multi-walled carbon nanotubes (MWCNT), fullerene.	541 (SWCNT); 94.7–348 (MWCNTs); 7.21 (fullerene).	$V_{pore, meso}$: 0.82 cm ³ g ⁻¹ (SWCNT); 0.22–0.69 cm ³ g ⁻¹ (MWCNTs); n.a. (fullerene). $V_{pore, micro}$: 0.20 cm ³ g ⁻¹ (SWCNT); 0.04–0.13 cm ³ g ⁻¹ (MWCNTs); 0.002 (fullerene)	$C_e = ca. 40 \text{ mg L}^{-1}$, $q_e = ca. 600 \text{ mg g}^{-1}$ (SWCNT, highest value reported).	455 mg g ⁻¹ (SWCNT, highest value)	A 7-day equilibrating period was used in sorption experiments.	Pan et al., 2008 ¹²
Graphene	Synthesized in laboratory	327	Not available	$C_e = ca. 32.5 \text{ mg L}^{-1}$, $q_e = ca. 175 \text{ mg g}^{-1}$ (highest value), at 29°C.	123.9–181.8 mg g ⁻¹ , at 29–69°C	Elevated temperatures (29–69°C) were used in sorption experiments.	Xu et al., 2012 ¹³
Zeolite	Zeolites, as-prepared and surfactant-modified.	91.5 (ZFA F, as-prepared)	Not available	$C_e = ca. 52 \text{ mg L}^{-1}$, $q_e = ca. 93 \text{ mg g}^{-1}$ (highest value, surfactant-modified ZFA F)	114.9 (highest value, surfactant-modified ZFA F)	The pH of equilibrium solutions was 9.6–11.2. BPA uptake was reduced by setting pH to 5.0 ± 0.1.	Dong et al., 2010 ¹⁴
ACs	Charcoal-based commercial ACs from Sorbo-Norit (3-A-7472) and Merck (K27350518015), as-received and HCl-treated, and one lab-prepared AC from almond shells.	1084–1277	$V_{pore, micro}$: 0.496–0.565	$C_e = ca. 75 \text{ mg L}^{-1}$, $q_e = ca. 250 \text{ mg g}^{-1}$ (highest value, Merck AC); $C_e = ca. 65 \text{ mg L}^{-1}$, $q_e = ca. 190 \text{ mg g}^{-1}$ (lab-prepared AC); $C_e = ca. 85 \text{ mg L}^{-1}$, $q_e = ca. 120 \text{ mg g}^{-1}$ (Sorbo-Norit AC)	263.1 (Merck AC); 188.9 (lab-prepared AC); 129.6 (Sorbo-Norit AC)	A 7-day equilibrating period was used for sorption isotherm experiments.	Bautista-Toledo et al., 2005 ¹⁵

Notes: Data tabulated above are the highest values reported in literature on BPA sorption capacities. Additional data at lower concentration ranges are available in the references cited in this table (Xu et al., 2012; Dong et al., 2010; Pan et al, 2008). Experimental data were graphically determined from figures presented in references and, although they represent our best estimates, errors may exist from our graph reading.

Table S4. BPA sorption by PUF, dvb-PS, and AC under high levels of co-existing humic acids (HAs)

	<i>Initial [BPA], mg L⁻¹</i>	<i>Initial [HAs], mg L⁻¹</i>	<i>Free [BPA] after sorption, μg L⁻¹</i>	<i>Free [HAs] after sorption, mg L⁻¹</i>
<i>PUF</i>	1.0	n.a. (control)	44.8 ± 1.8	n.a.
	1.0	20	43.5 ± 3.4	19.8 ± 0.2
	1.0	40	47.6 ± 2.2	37.6 ± 1.6
<i>dvb-PS</i>	1.0	n.a. (control)	n.d.	n.a.
	1.0	20	n.d.	19.4 ± 0.4
	1.0	40	n.d.	39.9 ± 0.1
<i>AC</i>	1.0	n.a. (control)	n.d.	n.a.
	1.0	20	n.d.	6.6 ± 0.1
	1.0	40	96.8 ± 5.8	23.2 ± 0.1

Notes: The large molecular sizes of humic acids can also cause pore-blocking effects in porous adsorbents and consequently affect their adsorption for BPA. This was not observed in Figure 4b due to the relatively high sorbent dosage used, but became evident in AC after further increasing the concentrations of co-existing humic acids to 20 and 40 mg L⁻¹. As shown in the table, both PUF and dvb-PS exhibited consistent sorption capacities for BPA and negligible sorption for co-existing HAs under the higher concentrations of HAs. In contrast, BPA sorption by AC decreased under the highest concentration of co-existing HAs, *i.e.* 40 mg L⁻¹ which represents the upper level of HAs in aquatic environments.¹⁶ This may be ascribed to the competitive sorption of HAs on AC or pore blocking effects caused by the large molecules of HAs, or a combination of both. Abbreviations in the table: HAs, humic acids; n.a., not applicable (pure BPA solutions were used in control experiments with no co-existing HAs); n.d., non-detectable by HPLC-UV, *i.e.* [BPA] < 1 μg L⁻¹.

Table S5. TOC analysis of the potential release of PUF monomers and oligomers

	<i>TOC measurements (raw data of peak areas)</i>										<i>BPA conc. by HPLC ($\mu\text{g L}^{-1}$)</i>	<i>TOC of BPA ($\mu\text{g L}^{-1}$)</i>
	<i>Meas. #1</i>	<i>Meas. #2</i>	<i>Meas. #3</i>	<i>Meas. #4</i>	<i>Meas. #5</i>	<i>Meas. #6</i>	<i>Meas. #7</i>	<i>Meas. #8</i>	<i>Avg.</i>	<i>Std Dev</i>		
<i>Deionized water (background)</i>	2.859	2.481	2.470	1.784	1.581	1.880	2.199	2.552	2.226	0.441	n.a.	n.a.
<i>KHP standard (50 $\mu\text{gC L}^{-1}$)^a</i>	2.227	2.863	2.126	2.537	2.731	2.218	2.503	2.808	2.502	0.287		
<i>KHP standard (100 $\mu\text{gC L}^{-1}$)^a</i>	3.058	2.735	3.344	2.641	2.692	3.051	2.681	3.155	2.920	0.265		
<i>KHP standard (500 $\mu\text{gC L}^{-1}$)^a</i>	6.542	6.728	6.680	6.967	6.492	6.608	6.559	6.826	6.608	0.269		
<i>KHP standard (1.0 mgC L^{-1})^a</i>	11.10	10.63	10.86	11.25	11.11	11.25	11.38	n.a.	11.08	0.258		
<i>KHP standard (10 mgC L^{-1})^a</i>	87.78	88.28	90.00	89.60	88.70	89.52	n.a.	n.a.	88.98	0.863		
<i>PUF rinsing water</i>	2.099	2.122	2.434	2.541	2.354	1.868	1.885	2.323	2.203	0.249		
<i>PUF-treated BPA solution^b</i>	2.592	2.417	2.162	2.625	2.010	2.327	2.005	1.776	2.239	0.302	54.6 \pm 0.4 ^c	43.1 \pm 0.3

Notes: TOC analysis was performed on a Shimadzu TOC-L Total Organic Carbon Analyzer using high-sensitivity catalyst under non-purgeable organic carbon (NPOC) mode. The instrument has a nominal detection limit of 4 $\mu\text{g L}^{-1}$ for organic carbons in water and a measured detection limit below 50 $\mu\text{g L}^{-1}$ under our settings (see results of the 50 $\mu\text{g L}^{-1}$ TOC standard). All glassware used in the sample preparation including sample vials, a volumetric flask (used for BPA sorption experiment), transfer pipettes, and a glass rod were washed, rinsed with deionized water, and ashed at 450°C for 2 h in a furnace to remove organic carbon residues before use. Notes: (a) The standard solution were prepared by accurately weighing 2.125 g of reagent-grade potassium hydrogen phthalate (KHP) and dissolving it into Barnstead™ NanoPure™ deionized water in a 1 L volumetric flask. The standard solution contained 1000 mgC L^{-1} and was further diluted into several lower concentration standards, *i.e.* 10, 1.0, 0.5, 0.1, and 0.05 mgC L^{-1} . (b) PUF was added into the BPA working solution at a dosage of 1.5 g L^{-1} and equilibrated for 24 h under agitation at room temperature. HPLC measurements determined that the initial BPA working solution contained 1.154 \pm 0.003 mg L^{-1} BPA and 54.6 \pm 0.4 $\mu\text{g L}^{-1}$ residual BPA (or 43.1 \pm 0.3 $\mu\text{gC L}^{-1}$) after PUF sorption. TOC measurements of the PUF-treated BPA solution showed no sign of increase compared to the results of 50 $\mu\text{gC L}^{-1}$ TOC standard, and were obviously lower than the results obtained on the 100 $\mu\text{gC L}^{-1}$ TOC standard. The results indicate that, within the detection capability of the TOC analysis, there was no detectable release of monomers or oligomers from PUF during the BPA sorption process. Similar results were obtained on PUF rinsing water sample, which showed similar TOC measurements as the Barnstead™ NanoPure™ deionized water background. The PUF rinsing water was obtained by immersing a pre-washed PUF block (0.15 g) in 100 mL Barnstead™ NanoPure™ deionized water and agitating the suspension for 24 h before collecting the sample. (c) The BPA concentration after PUF sorption represents the average result from triplicate HPLC measurements.

References

1. S. Azizian, Kinetic models of sorption: A theoretical analysis, *Journal of Colloid and Interface Science*, 276 (2004) 47–52.
2. Hitachi High Technologies, Hitachi S-4700 SEM Training & Reference Guide, January 2007, p16.
3. JA de Haseth, JE Andrews, JV McClusky, RD Priester, MA Harthcock, and BL Davis, Characterization of polyurethane foams by mid-infrared fiber/FT-IR spectrometry, *Applied Spectroscopy*, 47 (1993) 173–179.
4. P Larkin, Chapter 7: General outline and strategies for IR and Raman Spectral interpretation, in *Infrared and Raman Spectroscopy: Principles and Spectral Interpretation*, Elsevier, 2011.
5. KC Cole and P Van Gheluwe, Flexible polyurethane foam. I. FTIR Analysis of Residual Isocyanate, *Journal of Applied Polymer Science*, 34 (1987) 395–407.
6. A Shareef, MJ Angove, JD Wells, and BB Johnson, Aqueous solubilities of estrone, 17 β -estradiol, 17 α -ethynylestradiol, and bisphenol A, *Journal of Chemical & Engineering Data*, 51 (2006) 879–881.
7. Rohm and Haas (Dow Chemical), Amberlite XAD polymeric resins, Product information sheet. www.sigmaaldrich.com/content/dam/sigma-aldrich/docs/Sigma/Product_Information_Sheet/1/xad4pis.pdf
8. Norit Americas Inc., Darco® 12×20 Granular Activated Carbon, Dec 2004. www.reskemgw.com/pdf/norit-darco1220.pdf
9. Z Xu, Q Zhang, and HHP Fang, Applications of Porous Resin Sorbents in Industrial Wastewater Treatment and Resource Recovery, *Critical Reviews in Environmental Science and Technology*, 33 (2003) 363–389.
10. B Pan, B Pan, W Zhang, Lu Lv, Q Zhang, S Zheng, Development of polymeric and polymer-based hybrid adsorbents for pollutants removal from waters, *Chemical Engineering Journal*, 151 (2009) 19–29.
11. CY Kuo, Comparison with as-grown and microwave modified carbon nanotubes to remove aqueous bisphenol A, *Desalination*, 249 (2009) 976–982.
12. B Pan, D Lin, H Mashayekhi, and B Xing, Adsorption and Hysteresis of Bisphenol A and 17 α -Ethinyl Estradiol on Carbon Nanomaterials, *Environmental Science & Technology*, 42 (2008) 5480–5485.
13. J Xu, L Wang, and Y Zhu, Decontamination of Bisphenol A from Aqueous Solution by Graphene Adsorption, *Langmuir*, 28 (2012) 8418–8425.
14. Y Dong, D Wu, X Chen, Y Lin, Adsorption of bisphenol A from water by surfactant-modified zeolite, *Journal of Colloid and Interface Science*, 348 (2010) 585–590.
15. I Bautista-Toledo, MA Ferro-García, J Rivera-Utrilla, C Moreno-Castilla, and FJ Vegas Fernández, Bisphenol A removal from water by activated carbon. Effects of carbon characteristics and solution chemistry, *Environmental Science & Technology*, 39 (2005) 6246–6250.
16. FH Frimmel. Aquatic humic substances. In *Biopolymers Online*, Wiley-VCH, 2005. onlinelibrary.wiley.com/doi/10.1002/3527600035.bpol1010/full